Available online at www.sciencedirect.com
ScienceDirect
International Journal of Solids and Structures 44 (2007) 6080–6100
INTERNATIONAL JOURNAL OF SOLIDS AND STRUCTURES
www.elsevier.com/locate/ijsolstr

A constitutive model for cavitation and cavity growth in rubber-like materials under arbitrary tri-axial loading

J. Li [a,*], D. Mayau [b], F. Song [c]

[a] LPMTM, CNRS UPR 9001, Institut Galilée, Université Paris XIII, 99 Avenue Jean-Baptiste Clément, 93430 Villetaneuse, France
[b] TRELLEBORG Engineered System, ZI La Combaude - F-63050 Clermont-Ferrand, France
[c] LNM, Institute of Mechanics, Chinese Academy of Sciences, Beijing 100080, China

Received 20 February 2006; received in revised form 1 February 2007
Available online 13 February 2007

Abstract

In this paper, we attempted to construct a constitutive model to deal with the phenomenon of cavitation and cavity growth in a rubber-like material subjected to an arbitrary tri-axial loading. To this end, we considered a spherical elementary representative volume in a general Rivlin's incompressible material containing a central spherical cavity. The kinematics proposed by [Hou, H.S., Abeyaratne, R., 1992. Cavitation in elastic and elastic-plastic solids. J. Mech. Phys. Solids 40, 571–722] was adopted in order to construct an approximate but optimal field. In order to establish a suitable constitutive law for this class of materials, we utilized the homogenisation technique that permits us to calculate the average strain energy density of the volume. The cavity growth was considered through a physically realistic failure criterion. Combination of the constitutive law and the failure criterion enables us to describe correctly the global behaviour and the damage evolution of the material under tri-axial loading. It was shown that the present models can efficiently reproduce different stress states, varying from uniaxial to tri-axial tensions, observed in experimentations. Comparison between predicted results and experimental data proves that the proposed model is accurate and physically reasonable. Another advantage is that the proposed model does not need special identification work, the initial Rivlin's law for the corresponding incompressible material is sufficient to form the new law for the compressible material resulted from cavitation procedure.
© 2007 Elsevier Ltd. All rights reserved.

Keywords: Rubber; Compressible materials; Cavitation; Cavity growth; Homogenization; Damage; Fracture

1. Introduction

The phenomenon of cavitation and cavity growth in rubber-like materials was observed long time ago. Gent and Lindley (1958) (see also Williams and Schapery, 1965) carried out a tensile test on a flat cylinder rubber sheet between two metal plates to generate a highly tri-axial stress state in the central part of the specimen. The force–displacement curves exhibit a break point corresponding to the creation of cavities. These

* Corresponding author. Tel.: +33 1 49 40 28 89; fax: +33 1 49 40 39 38.
E-mail address: jia.li@lpmtm.univ-paris13.fr (J. Li).

0020-7683/$ - see front matter © 2007 Elsevier Ltd. All rights reserved.
doi:10.1016/j.ijsolstr.2007.02.016

cavities then grow as the load increases until the specimen's final fracture. This phenomenon was confirmed by numeral experimental studies latter (Lindsey, 1967; Kakavas and Chang, 1991, 1992; Bathias et al., 1996; Dorfmann and Burtscher, 2000; Legorju-jago and Bathias, 2002; Dorfmann, 2003). This phenomenon implies that the conventional incompressible constitutive laws, usually utilized in modelling rubber-like materials under uniaxial or biaxial loading, are no longer applicable if the tri-axiality reaches a certain level. Compressibility has to be introduced to consider such a case.

Two distinguish approaches can be found in the literature to model the cavitation phenomenon in rubbers. The first one is to adopt phenomenological compressible constitutive laws. In this kind of approaches, the strain energy density, which can be considered as the basic function characterizing the material behaviours, is often split into two parts: the first part describes usually the incompressible behaviour while the second describes the compressible one. The incompressible part of the strain energy density was thoroughly studied, the most widely cited strain energy expressions are the Money-Rivlin, Ogden (1972) and Arruda and Boyce (1993) models amongst many others. These models in general can describe properly the rubber behaviours in uniaxial or biaxial stress states. However, the compressible part of the strain energy has not well studied so far. In general, the compressible term in the energy density is often considered as function of volume changes. For fixed porosities, various forms of compressible laws can be found in Ogden (1972, 1976). A popular compressibility law proposed by Blatz and Ko (1962) is also widely used in engineering applications. Some more elaborated compressibility laws were proposed by Simo and Pister (1984), Bischoff et al. (2000) and Attard and Hunt (2002) among others.

A critic that one can make to these phenomenological compressibility laws is the lack of physical basis. The separable form of the strain energy function is often adopted just because of its mathematical convenience. Therefore, the performance of this class of models is sometimes limited within a low level of compressibility.

The second approach in modelling the cavitation and cavity growth is to study the cavities in an incompressible medium. The global behaviours of the voided materials exhibit compressibility. It is clear that this approach benefits from its realistic physical foundation. Ball (1982) proposed a mathematical analysis of the stability conditions for the case of a spherical cavity under purely hydrostatic loading. He showed that for a particular class of material behaviour laws, there exists a bifurcated solution that corresponds to the cavity nucleation. In the special case of a neo-Hookean material, the theoretical critical stress for cavitation thus determined has good agreement with the experimental results of Gent and Lindley (1958). An alternative interpretation of cavitation instability in terms of the growth of a pre-existing micro-void was given by Horgan and Abeyaratne (1986). After that numerous studies in this direction, essentially dealing with spherical or cylindrical cavities subjected to symmetrical radial tension, were given by different authors (Biva, 1995; Ganghoffer and Schultz, 1995; Shang and Cheng, 2001; Chang and Pan, 2001; Hou and Zhang, 1992; Polignone and Horgan, 1993; etc.).

When a solid is subjected to an arbitrary tri-axial loading, the exact bifurcated solution is rather difficult to find out, even for the simplest neo-Hookean constitutive law. Hou and Abeyaratne (1992) considered a prescribed cinematically admissible three-dimensional deformation fields for a central spherical cavity under global tri-axial tension, such that the deformation carries the spherical cavity into an ellipsoidal one. By applying the principle of virtual work, a cavitation surface in the space of principal true stresses was found for neo-Hookean materials. This analysis was extended to a composite consisting of concentric spheres of neo-Hookean materials by Steenbrink and Van der Giessen (1999) in their studies on polymer-rubber blends.

Apart from the cavity nucleation prediction, another important issue in this topic is the cavity growth evaluation under tri-axial loading. In the phenomenological models, the cavity growth represents one of the damage responses of rubber-like materials. One can cite the works of Ogden and Roxburgh (1999) and Dorfmann et al. (2002) who proposed the so-called pseudo-elasticity theory, in which the material response is described by different forms of strain energy density on primary loading and subsequent unloading. This theory was applied to assess the cavitation damage (Dorfmann et al., 2002) with success in the case of relatively small values of deformation. On the other hand, many studies were focused on the inner surface tearing of the cavity. A currently accepted criterion is the maximum chain stretch criterion, stating that a rubber chain can be broken only when it is fully extended. A similar criterion is based on the equi-biaxial stress state on the inner cavity boundary under hydrostatic tension (Chang and Pan, 2001). In all these criteria, the cavity begins to

grow when a strain variable on the cavity's inner boundary reaches a critical level. Another group of cavity growth criteria are established on the basis of energy balance. Williams and Schapery (1965) proposed using Griffith's formulation to model irreversible expansion of a spherical cavity. This concept was extended by Gent and Wang (1991), Fond et al. (1996) and Diani (1999). It is to notice that this criterion was only applied to the case of a spherical cavity in neo-Hookean materials.

In summery, our bibliographical research shows that the cavitation and cavity growth in rubbers have not been thoroughly studied so far. Since the industrial applications we encountered require also the solution of such problems, combination of these facts motivate us to perform a detailed study on this topic.

In this paper, we attempted to establish a family of new constitutive models for rubber-like materials that are suitable not only for uniaxial and biaxial loading cases, but also for tri-axial tensions. The basic idea is to consider an elementary cell in a general Rivlin's incompressible material containing a central spherical cavity and subjected to a general tri-axial tension. The kinematics proposed by Hou and Abeyaratne (1992) was adopted in order to construct an approximate but optimal field. On the one hand, we performed a homogenisation analysis on this elementary volume on the basis of this kinematics. On the other hand, we proposed a physically realistic failure criterion to assess the cavity growth phenomenon. It must be noted that the existence of initial porosity may not be the only source of the cavitation, but other aspects were not considered in this work. The constitutive models thus established were therefore examined by considering simple specific stress states. This constitutive model was implemented into a finite element program that was used to model more complicate experimentations. Comparison between the results predicted by the present model and the experimental data show that the present models can efficiently reproduce different stress states including uniaxial, biaxial and tri-axial tensions. The concept proposed is simple and easy to apply into engineering calculations. Afterwards, the accuracy and the possibility of improvement of the models are discussed. Finally, some concluding remarks are given at the end of this paper.

2. Preliminaries

Before describing the present model for compressible rubber-like materials, we first recall the different notations used in the present study.

We consider a rubber-like solid as a continuous body. A material point M occupies a position $\boldsymbol{X}$ at the initial time (at unstressed configuration), and a position $\boldsymbol{x}$ at the current time (at stressed current configuration). In Cartesian coordinate system, $\boldsymbol{X}$ and $\boldsymbol{x}$ have, respectively, coordinate X_i and x_i, $i = 1, 2, 3$. The movement of the point M can be described by a second order tensor, the deformation gradient tensor $\boldsymbol{F}$, given by $\boldsymbol{F} = \mathrm{Grad}\boldsymbol{x}$ with Cartesian components $F_{ij} = \frac{\partial x_i}{\partial X_j}$, Grad being the gradient operator with respect to $\boldsymbol{X}$. When the material is incompressible, we have $\det\boldsymbol{F} = 1$. The deformation gradient can be decomposed according to the polar decompositions $\boldsymbol{F} = \boldsymbol{R}\boldsymbol{U} = \boldsymbol{V}\boldsymbol{R}$, where $\boldsymbol{R}$ is an orthogonal rotational tensor. $\boldsymbol{U}$ and $\boldsymbol{V}$ are symmetric and positive definite tensors. Consider the tensor $\boldsymbol{U}$ for example, let λ_i be the eigenvalues of $\boldsymbol{U}$ and $\boldsymbol{u}_i$ its unit eigenvectors, $\boldsymbol{U}$ can be expressed as

$$\boldsymbol{U} = \sum_{i=1}^{3} \lambda_i \boldsymbol{u}_i \otimes \boldsymbol{u}_i. \tag{1}$$

It is clear that λ_i are the principal stretches and $\lambda_i > 0$. Associated to $\boldsymbol{U}$ and $\boldsymbol{V}$, the commonly used strain tensors are:

$$\text{The left Cauchy–Green stretch tensor} : \boldsymbol{B} = \boldsymbol{V}^2 = \boldsymbol{F}\boldsymbol{F}^{\mathrm{T}} \tag{2}$$

$$\text{The right Cauchy–Green stretch tensor} : \boldsymbol{C} = \boldsymbol{U}^2 = \boldsymbol{F}^{\mathrm{T}}\boldsymbol{F} \tag{3}$$

$$\text{The Cauchy–Lagrange strain tensor} : \boldsymbol{E} = \frac{1}{2}(\boldsymbol{C} - \boldsymbol{I}) \tag{4}$$

In the theory of hyperelasticity, one supposes that there exists a strain energy density function W. The constitutive laws of a hyperelastic material can be represented via this function by means of different stress tensors, namely

$$\text{The Boussinesq stress tensor } \boldsymbol{\Pi} = \frac{\partial W}{\partial \boldsymbol{F}} \tag{5}$$

$$\text{The Biot stress tensor } \boldsymbol{T} = \frac{\partial W}{\partial \boldsymbol{U}} = \boldsymbol{\Pi}\boldsymbol{R}^{\mathrm{T}} \tag{6}$$

$$\text{The second Piola-Kirchhof stress tensor : } \boldsymbol{S} = \frac{\partial W}{\partial \boldsymbol{E}} \tag{7}$$

$$\text{The Cauchy stress tensor : } \boldsymbol{\sigma} = \frac{1}{J}\boldsymbol{F}\boldsymbol{\Pi} = \frac{1}{J}\boldsymbol{F}\boldsymbol{S}\boldsymbol{F}^{\mathrm{T}} \tag{8}$$

Generally speaking, the Biot stress tensor $\boldsymbol{T}$ is more convenient to describe the simple stress states occurred in commonly defined experimental protocols since it represents the nominal engineering stresses in the principal stretch directions. While in finite element analyses, the use of the second Piola–Kirchooff stress tensor $\boldsymbol{S}$ is more suitable. These stress tensors can be converted into the Cauchy stress tensor $\boldsymbol{\sigma}$, or the true stress tensor, that gives a more physical interpretation of the interior forces in the body. For these reasons, the constitutive relations issued from (6) and (7) were essentially used in the present study.

3. Basic considerations

In this section, we describe the establishment of the model in dealing with a compressible porous elastomer. The main idea is to consider an elementary representative volume in an incompressible rubber-like material containing a central cavity. We believe that the homogenisation of this elementary volume associated to a physically realistic failure criterion would be able to correctly describe the global behaviour of the material under tri-axial loading.

3.1. Homogenization procedure

A Voigt-type homogenization procedure (1889) was used in order to establish a constitutive model being capable to take into account the compressibility induced by cavities. Let Ω be a sphere occupied by an unstressed incompressible elastomer. Its volume is supposed to be unit, with its initial external radius $b_0 = (3/4\pi)^{1/3}$. We assume the existence in Ω of a centered spherical void of radius a_0. In general, the initial porosity of the material is assumed to be weak, i.e., $a_0 \ll b_0$. This assumption permits to deduce that there is no interacting effect between cavities. As a consequence, Ω can be considered as a representative elementary volume (REV) extracted from a real elastomer body. Suppose that its boundary is subjected to a uniform traction $\overline{\boldsymbol{T}} = \overline{T}_1 N_1 \boldsymbol{e}_1 + \overline{T}_2 N_2 \boldsymbol{e}_2 + \overline{T}_3 N_3 \boldsymbol{e}_3$, where $\overline{\boldsymbol{T}}$ is the *nominal* traction vector, $\boldsymbol{e}_i$ $(i = 1,2,3)$ are the unit vectors of a fixed orthonormal basis, N_i $(i = 1,2,3)$ are the components of the unit outward normal vector at a point on the undeformed boundary. Ω being a small volume, we assume that $\overline{T}_i$ $(i = 1,2,3)$ are constant on its outer boundary. It is clear that the vector $\overline{\boldsymbol{T}}$ just corresponds to the principal values of the Biot stress tensor $\boldsymbol{T}$.

In the spherical coordinate system (R, Θ, Φ), the position of a point in Ω is written as follows:

$$X_1 = R\cos\Theta \quad X_2 = R\sin\Theta\cos\Phi \quad X_3 = R\sin\Theta\sin\Phi \qquad (a_0 \leqslant R \leqslant b_0,\ 0 \leqslant \Theta \leqslant \pi,\ 0 \leqslant \Phi \leqslant 2\pi) \tag{9}$$

Hou and Abeyaratne (1992) supposed that the deformation of such a volume in response of the prescribed loading can be approximated by a three-parameter family kinematics of the following form:

$$x_1 = \bar{\alpha}_1\psi(R)X_1 \quad x_2 = \bar{\alpha}_2\psi(R)X_2 \quad x_3 = \bar{\alpha}_3\psi(R)X_3 \tag{10}$$

where $\bar{\alpha}_1$, $\bar{\alpha}_2$ and $\bar{\alpha}_3$ are positive unknown constants satisfying $\bar{\alpha}_1\bar{\alpha}_2\bar{\alpha}_3 = 1$ and

$$\psi(R) = \left(1 + \frac{\beta^3}{R^3}\right)^{\frac{1}{3}} \tag{11}$$

where $\beta \geqslant 0$. This kinematics implies that an initially spherical volume becomes ellipsoidal after deformation.

By adopting this kinematics, a point on the deformed boundary of Ω becomes

$$x_i = \bar{\alpha}_i\psi(b_0)X_i = \bar{\lambda}_i X_i \quad i = 1,2,3 \tag{12}$$

where $\bar{\lambda}_i = \bar{\alpha}_i \psi(b_0)$ are the apparent stretches observed on the exterior boundary of Ω. In the sense of the homogenization, it can be considered as the uniform stretches in the homogenized body. The displacement of a point on the boundary is therefore:

$$u_i = x_i - X_i = (\bar{\lambda}_i - 1)X_i \quad i = 1, 2, 3. \tag{13}$$

The work performed by the external traction can be written as:

$$\begin{aligned} W_{\text{ext}} &= \int_A \overline{T}_i u_i \mathrm{d}A \\ &= \int_0^{2\pi} \int_0^{\pi} b_0 \big(\overline{T}_1(\bar{\lambda}_1 - 1)\cos^2\Theta + \overline{T}_2(\bar{\lambda}_2 - 1)\sin^2\Theta\cos^2\Phi + \overline{T}_3(\bar{\lambda}_3 - 1)\sin^2\Theta\sin^2\Phi\big) b_0^2 \sin\Theta \mathrm{d}\Theta\mathrm{d}\Phi \\ &= \overline{T}_1(\bar{\lambda}_1 - 1) + \overline{T}_2(\bar{\lambda}_2 - 1) + \overline{T}_3(\bar{\lambda}_3 - 1), \end{aligned} \tag{14}$$

where A is the outer boundary surface area of the undeformed sphere. The deformation energy stored in the body can be obtained by:

$$\overline{W} = \int_\Omega W \mathrm{d}\Omega, \tag{15}$$

where W is the strain energy density in Ω. According to the principle of virtual work, the equilibrium of the body requires $\delta\overline{W} = \delta W_{\text{ext}}$. This argument leads to write:

$$\delta\overline{W} = \overline{T}_1\delta\bar{\lambda}_1 + \overline{T}_2\delta\bar{\lambda}_2 + \overline{T}_3\delta\bar{\lambda}_3. \tag{16}$$

Consequently, we obtain:

$$\overline{T}_i = \frac{\partial\overline{W}}{\partial\bar{\lambda}_i} \quad i = 1, 2, 3. \tag{17}$$

Since Ω is a unit volume, therefore $\bar{W}$ can be considered as the average strain energy density in a porous elastomer body. Similarly, $\overline{T}_i$ and $\bar{\lambda}_i$ can, respectively, be considered as the average Biot principal stresses and the apparent stretches. Comparing (17) to (6), we can see that the constitutive relationships are formally identical in a homogenized porous elementary representative volume with those in a homogeneous hyperelastic body. In the case when the kinematics chosen in (10) is such that the coordinate axes do not coincide with the principal stretch directions, following the same homogenization procedure described above will lead to write:

$$\overline{\boldsymbol{T}} = \frac{\partial\overline{W}}{\partial\overline{\boldsymbol{U}}}, \tag{18}$$

where $\overline{\boldsymbol{T}}$ and $\overline{\boldsymbol{U}}$ are, respectively, the average Biot stress tensor and the apparent stretch tensor measured on the exterior boundary of Ω. Consequently, once the average strain energy density $\overline{W}$ is known for a porous elastomer, the homogenized constitutive laws can identically be obtained from standard constitutive relationships of a hyperelastic material.

3.2. Average strain energy density in the elementary cell

Now let us evaluate the average strain energy $\overline{W}$ in a porous elastomer body. The initial porosity of the body Ω is defined as

$$f_0 = \frac{a_0^3}{b_0^3}. \tag{19}$$

According to (11) and (12), we can calculate the volume expansion of Ω

$$J = \bar{\lambda}_1\bar{\lambda}_2\bar{\lambda}_3 = \bar{\alpha}_1\bar{\alpha}_2\bar{\alpha}_3\psi^3(b_0) = 1 + \frac{\beta^3}{b_0^3}, \tag{20}$$

and the expansion of the cavity

$$J_a = \bar{\alpha}_1\bar{\alpha}_2\bar{\alpha}_3\psi^3(a_0) = 1 + \frac{\beta^3}{a_0^3}. \tag{21}$$

The porosity of the deformed body is:

$$f = \frac{J_a a_0^3}{J b_0^3} = \frac{a_0^3 + \beta^3}{b_0^3 + \beta^3}. \tag{22}$$

Now let us define the following parameters:

$$b^3 = b_0^3 + \beta^3 \qquad a^3 = a_0^3 + \beta^3, \tag{23}$$

it is clear that

$$\frac{b^3}{b_0^3} = J \qquad \frac{a^3}{a_0^3} = 1 + \frac{J-1}{f_0}. \tag{24}$$

The porosity of the deformed body can therefore be written as function of the initial porosity and the volume change ratio:

$$f = \frac{f_0}{J}\left(1 + \frac{J-1}{f_0}\right). \tag{25}$$

By keeping these parameters in mind, we now turn to the evaluation of the stored strain energy in Ω when this one is subjected to a tri-axial deformation. The elastomer body being considered as incompressible, we can suppose that its behaviour can be represented by a general Rivlin's law with appropriately adjusted parameters C_{kl}:

$$W(I_1, I_2) = \sum_{k=0}^{K}\sum_{l=0}^{L} C_{kl}(I_1 - 3)^k (I_2 - 3)^l, \tag{26}$$

where I_1 and I_2 are the first and the second invariants of the right Cauchy–Green stretch tensor $\boldsymbol{C}$, namely

$$I_1 = \mathrm{tr}\boldsymbol{C} \quad I_2 = \frac{1}{2}\left(I_1^2 - \mathrm{tr}\boldsymbol{C}^2\right). \tag{27}$$

For the kinematics described by (10), the invariants I_1 and I_2 have the following form (Hou and Abeyaratne, 1992):

$$\begin{aligned} I_1 &= \psi^2\left(\bar{\alpha}_1^2 + \bar{\alpha}_2^2 + \bar{\alpha}_3^2\right) + \frac{1}{R^2}\left(\psi^{-4} - \psi^2\right)\left(\bar{\alpha}_1^2 X_1^2 + \bar{\alpha}_2^2 X_2^2 + \bar{\alpha}_3^2 X_1^2\right) \\ I_2 &= \psi^{-2}\left(\bar{\alpha}_1^{-2} + \bar{\alpha}_2^{-2} + \bar{\alpha}_3^{-2}\right) + \frac{1}{R^2}\left(\psi^4 - \psi^{-2}\right)\left(\bar{\alpha}_1^{-2} X_1^2 + \bar{\alpha}_2^{-2} X_2^2 + \bar{\alpha}_3^{-2} X_1^2\right). \end{aligned} \tag{28}$$

By substituting (26) into (15), the total strain energy in the body Ω can be written as follows:

$$\overline{W} = \int_{a_0}^{b_0}\int_0^{2\pi}\int_0^{\pi}\left[\sum_{k=0}^{K}\sum_{l=0}^{L} C_{kl}(I_1 - 3)^k (I_2 - 3)^l\right] R^2 \sin\Theta \mathrm{d}\Theta \mathrm{d}\Psi \mathrm{d}R. \tag{29}$$

Since Ω is a unit volume, (29) can also be considered as the average strain energy. Integration of this expression provides a constitutive law for a porous elastomer on the basis of the Hou–Abeyaratne kinematics. In general, the integral operation, event though presenting no specific difficulties, is rather fastidious. The explicit expression obtained is lengthy. Consequently, we do not attempt to obtain a general explicit expression of (29). Let us consider a five-term truncated Rivlin's law:

$$W(I_1, I_2) = C_{10}(I_1 - 3) + C_{01}(I_2 - 3) + C_{20}(I_1 - 3)^2 + C_{02}(I_2 - 3)^2 + C_{11}(I_1 - 3)(I_2 - 3), \tag{30}$$

the following truncated expression of (29) can be obtained, namely:

$$\overline{W} = C_0(1-f_0) + C_1\Phi_1 J_1 + C_2\Phi_2 J_2 + C_{20}\left[(\Phi_2+3\Phi_3)J_1^2 - 4\Phi_3 J_2\right] + C_{02}\left[(\Phi_1+3\Phi_4)J_2^2 - 4\Phi_4 J_1\right] + C_{11}[\Phi_5 J_1 J_2 + \Phi_6], \tag{31}$$

where C_0, C_1 and C_2 are constants resulted from the linear combination of the constants C_{kl} in (30); $\Phi_i(f_0,\bar{I}_3)$ are functions issued from integration, depending on the initial porosity f_0 and the volume change; J_1 and J_2 are, respectively, the first and the second average isochoric invariants, i.e.,

$$J_1 = \bar{I}_1\bar{I}_3^{-\frac{1}{3}}, J_2 = \bar{I}_2\bar{I}_3^{-\frac{2}{3}}, \tag{32}$$

$\bar{I}_1$, $\bar{I}_2$ and $\bar{I}_3$ are the average invariants defined by

$$\bar{I}_1 = \bar{\lambda}_1^2+\bar{\lambda}_2^2+\bar{\lambda}_3^2 \quad \bar{I}_2 = \bar{\lambda}_1^2\bar{\lambda}_2^2+\bar{\lambda}_2^2\bar{\lambda}_3^2+\bar{\lambda}_3^2\bar{\lambda}_1^2 \quad \bar{I}_3 = \bar{\lambda}_1^2\bar{\lambda}_2^2\bar{\lambda}_3^2. \tag{33}$$

It is clear that $J=\sqrt{\bar{I}_3}$, therefore, we can also write $\Phi_i(f_0,\bar{I}_3)\equiv\Phi_i(f_0,J)$. The expressions of C_i and $\Phi_i(f_0,J)$ are given in Appendix A.

3.3. Cavity evolution law

The analysis above-presented allows evaluation of rubber deformation for a fixed porosity in a rubber-like material under tri-axial loading. However, the cavities may grow if the loads reach a critical level. Therefore, in order to take this fact into account, criteria for the porosity evolution have to be established.

One can find different rubber failure criteria in the literature. In this work, we adopt the maximum chain stretch criterion in the evaluation of the cavity growth. Suppose that an ideal chain in the rubber network has n links. The maximum chain stretch criterion states that the chain can be broken only when it is fully extended. According to the statistic theory of rubber chains (see for examples, Treloar, 1975; Mark and Erman, 1988), this criterion yields:

$$I_{1\max} \leqslant 3n. \tag{34}$$

In the case of cavity growth problems, the maximum values of I_1 occur on the inner boundary of the cavity $R=a_0$, namely:

$$I_{1\max} \in I_1(R=a_0) = \psi^2(a_0)J_1 + \left(\psi^{-4}(a_0)-\psi^2(a_0)\right)\left[(\bar{\alpha}_1\cos\Theta)^2 + (\bar{\alpha}_2\sin\Theta\cos\Phi)^2 + (\bar{\alpha}_3\sin\Theta\sin\Phi)^2\right] \tag{35}$$

with

$$\psi(a_0) = \left(1+\frac{J-1}{f_0}\right)^{\frac{1}{3}}, \tag{36}$$

J_1 in (35) is the average first isochoric invariant defined in (32).

In the coordinate frame of the principal stretches, $I_{1\max}$ must occur at one of the principal axis. Since

$$I_1(X_i=a_0, X_j=0, i\neq j) = \psi^2(a_0)J_1 + \left(\psi^{-4}(a_0)-\psi^2(a_0)\right)\bar{\alpha}_i^2 \tag{37}$$

we have

$$I_{1\max} = \psi^2(a_0)J_1 + \left(\psi^{-4}(a_0)-\psi^2(a_0)\right)\min(\bar{\alpha}_i^2) \approx \psi^2(a_0)\left[J_1 - \min(\bar{\alpha}_i^2)\right] \leqslant 3n. \tag{38}$$

Here $\psi^{-4}(a_0)$ is neglected because a is much larger than a_0 at chain failure. Combining (36) and (38) yields:

$$g(\bar{\lambda}_1,\bar{\lambda}_2,\bar{\lambda}_3) \equiv \frac{J-1}{\Lambda J-1} - f_0 \leqslant 0 \tag{39}$$

with

$$\Lambda = \left[\frac{3n}{\bar{I}_1 - \min(\bar{\lambda}_i^2)}\right]^{\frac{3}{2}}. \tag{40}$$

Eq. (39) is the porosity evolution surface in the principal stretch space. In the case when $g < 0$, there is no evolution of the porosity. The case of $g > 0$ is physically unattainable. If this is the case, new porosity will be reached such that the inequality $g \leqslant 0$ always holds. If this inequality cannot be achieved, there will be an unstable cavity growth leading to a catastrophic failure.

From (40), we can observe that Λ decreases as $\bar{I}_1$ increases. Its possible minimal value is $\Lambda = 1$, because according to (39), this value leads to $f_0 = 1$, meaning that Ω is completely empty.

In this porosity evolution criterion, the chain length n is an important parameter. According to (34), it can be interpreted as the critical stretch value producing the chain break. It is clear that rubbers can withstand larger deformations as n increases. Consequently, a large n will also enable rubbers to resist better the cavity growth under tri-axial loading.

In this section, we have constructed a model for porous elastomers including a homogenized constitutive law for elastomers with cavities and a cavity evolution criterion. The application of this model can be described as follows: An initial porosity, even though very small, must be previously specified for the considered material. The constitutive behaviour of such a compressible material can therefore be described by the average strain energy density (31). Using this homogenized strain energy, the stress–stretch relationship can directly be obtained by derivations according to Eqs. (5)–(8). For an incremental loading step, the new porosity is evaluated according to the criterion (39). The porosity in the deformed body can be calculated from (25).

Since hereafter we only consider the homogenized body with the average quantities, we will *remove the overbars for symbols in all the constitutive equations* in order to simplify the notation.

4. Tri-axial model issued from the neo-Hookean law

The average strain energy density obtained from general Rivlin's law are often of complicated and lengthy form. In order to assess the capacity of the present model, we will first choose the simplest one issued from the neo-Hookean law for a detailed examination.

By taking into account only a single term in (30) and by replacing C_{10} by $\mu/2$, where μ is the shear module, we obtain:

$$W = \frac{3}{2}\mu(f_0 - 1) + \frac{1}{2}\mu\varphi(f_0, J)\left(\lambda_1^2 + \lambda_2^2 + \lambda_3^2\right) \tag{41}$$

with

$$\varphi(f_0, J) = (2 - J^{-1}) - f_0\left(J^2 + \frac{J^3 - J^2}{f_0}\right)^{-\frac{1}{3}}\left(1 + 2\frac{J-1}{f_0}\right). \tag{42}$$

In the case of incompressible materials, we have $J = 1$ and $f_0 = 0$, and this energy function is degenerated to the standard neo-Hookean law. The efficiency of this homogenized strain energy density in modelling rubber tri-axial deformation can be assessed by several specific strain states.

4.1. Uniaxial tension

In uniaxial tension, let λ_1 be the first average principal stretch in the direction of tension, we can calculate the nominal stress from (6), namely $T_1 = \partial W/\partial\lambda_1$, $T_2 = T_3 = \partial W/\partial\lambda_2 = 0$, these conditions lead to write:

$$\begin{aligned} T_1 &= \frac{\mu}{2}\frac{\mathrm{d}\varphi}{\mathrm{d}J}\lambda_2^2\left(\lambda_1^2 + \lambda_2^2 + \lambda_3^2\right) + \mu\varphi\lambda_1, \\ 0 &= \frac{\mu}{2}\frac{\mathrm{d}\varphi}{\mathrm{d}J}\lambda_1\lambda_2\left(\lambda_1^2 + \lambda_2^2 + \lambda_3^2\right) + \mu\varphi\lambda_2, \end{aligned} \tag{43}$$

with

$$\frac{\mathrm{d}\varphi}{\mathrm{d}J} = J^{-2} + f_0\frac{1}{3}\left(J^2 + \frac{J^3 - J^2}{f_0}\right)^{-\frac{4}{3}}\left(2J + \frac{3J^2 - 2J}{f_0}\right)\left(1 + 2\frac{J-1}{f_0}\right) - 2\left(J^2 + \frac{J^3 - J^2}{f_0}\right)^{-\frac{1}{3}}. \tag{44}$$

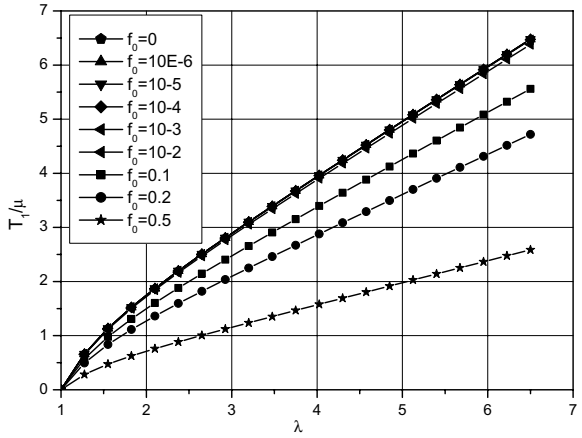

Fig. 1. Neo-Hookean laws for uniaxial tension with different fixed porosities f_0.

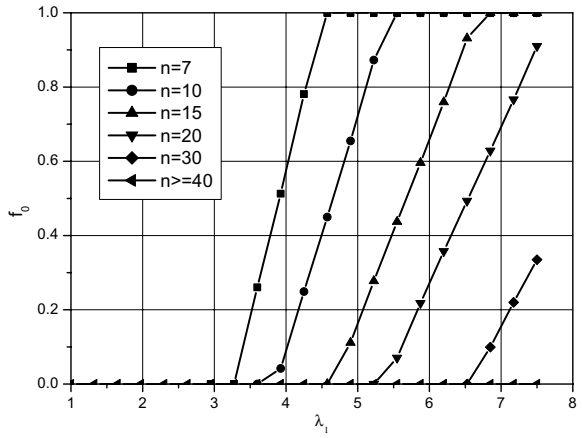

Fig. 2. Evolution of the porosity f_0 for different n under uniaxial tension.

From (43), we can eliminate $\lambda_2 = \lambda_3$ and deduce the relationship $T_1 = T_1(\lambda_1, f_0)$ by using numerical methods. Fig. 1 shows this relationship for different fixed initial porosities f_0. From this figure, we can remark that the $T_1 - \lambda_1$ curves for $f_0 \leqslant 0.01$ are practically identical to that of an incompressible material $f_0 = 0$. The difference from the incompressible neo-Hookean law is discernible only for very large porosities.

According the porosity evolution criterion established in this work, i.e., Eq. (39), we calculate the variation of f_0 during a uniaxial tension. From (39) and (40), we can see that the evolution of f_0 depends on the material parameter n, which represents the number of links in a rubber chain. In Fig. 2, we represent this evolution for an initially small porosity $f_0 = 10e{-}5$ versus axial stretch λ_1 for different values of n. The results of this calculation show that f_0 remains nearly unchanged until a critical value, and then it increases rapidly. From Fig. 2, we observe a clear dependency of the critical stretch, at which the porosity increases dramatically, on the parameter n: the critical stretch increases as n increases.

From the calculations described in this paragraph, we can suggest that the incompressible materials laws would be a good approximation for porous materials under uni-axial tension when the initial porosity level is not very high.

4.2. Equi-biaxial tension

In equi-biaxial tension, let$\lambda_1 = \lambda_2$ and we have $T_1 = T_2 = \partial W/\partial\lambda_1$ and $T_3 = \partial\ W/\partial\lambda_3 = 0$. Explicitly,

$$T_1 = \frac{\mu}{2}\frac{\mathrm{d}\varphi}{\mathrm{d}J}\lambda_1\lambda_3\left(\lambda_1^2+\lambda_2^2+\lambda_3^2\right)+\mu\varphi\lambda_1,$$
$$0 = \frac{\mu}{2}\frac{\mathrm{d}\varphi}{\mathrm{d}J}\lambda_2^2\left(\lambda_1^2+\lambda_2^2+\lambda_3^2\right)+\mu\varphi\lambda_3. \tag{45}$$

These equations allow the determination of stress-elongation relationships $T_1-\lambda_1$, as shown in Fig. 3. Here again, different fixed values of initial porosity were introduced in the calculation of $T_1-\lambda_1$ curves. Similar to the case of the uniaxial tension, only very large values of f_0 ($\geqslant 0.01$) can significantly modify the incompressible law.

The porosity evolution in this stress state was calculated according to the criterion (39) and illustrated in Fig. 4. If the parameter n is large enough, we can observe that f_0 remains at a weak level ($f_0 \leqslant 10\mathrm{e}{-5}$) for a large range of strains. This is quite a similar property to that observed in the case of uniaxial tension.

The analyses above-performed show that the present compressibility model coincides with the conventional incompressible theories in the cases of uniaxial and biaxial stress states if the initial porosity is weak. It reflects the fact that the cavity growth is not the principal damage mode for rubbers under this kind of loads and therefore the porosity does not develop significantly. Consequently, parameters in the present constitutive law can directly be determined by using the corresponding incompressible Rivlin's law.

Other biaxial strain states such as the pure shear exhibit similar properties and will not be discussed here.

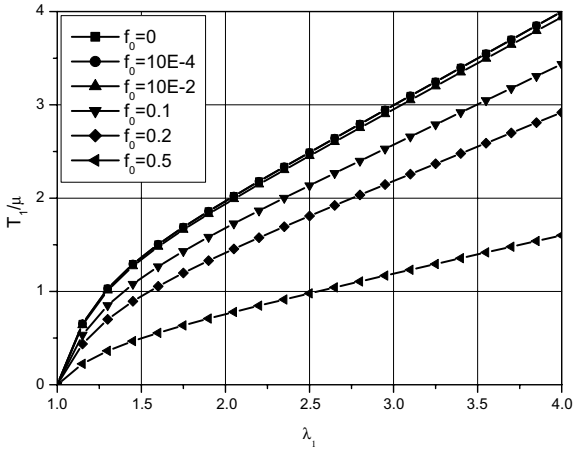

Fig. 3. Neo-Hookean laws for equi-biaxial tension with different fixed porosities f_0.

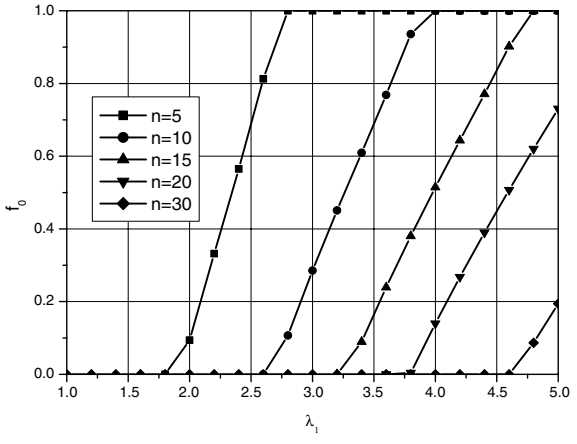

Fig. 4. Evolution of the porosity f_0 for different n under equi-biaxial tension.

4.3. Hydrostatic tension

The pure hydraulic tension is characterized by $\lambda_1 = \lambda_2 = \lambda_3$. The engineering nominal stress $T_1 = T_2 = T_3$ is obtained by

$$T_1 = \frac{\mu}{2}\frac{\mathrm{d}\varphi}{\mathrm{d}J}3\lambda_1^5 + \mu\varphi\lambda_1 \tag{46}$$

The relationships $T_1 - \lambda_1$ for different fixed f_0 were calculated and plotted in Fig. 5. From this figure, we can clearly observe that contrarily to the cases of uniaxial and biaxial tensions, the relationships $T_1 - \lambda_1$ depend strongly upon the initial porosity. First, the constitutive relations for small porosities mark a very rapid raising at the beginning of the curves, followed by gentler slopes. For very small f_0, we have $T_1(\lambda_1 \to 1) \to 2.5\mu$, which corresponds to the well-known cavitation pressure deduced by Ball (1982).

Using the cavity growth criterion (39), we can also draw the $T_1 - \lambda_1$ curves for growing porosity. In this case, we consider an infinitesimal initial porosity (for example, $f_0 = 10^{-9}$). The $T_1 - \lambda_1$ curves obtained using different values of n were plotted in Fig. 6. First, these curves exhibit a break point at $\lambda_1 \to 1$, corresponding to a rapid cavity growth. According to the values used of n, these curves present different progression slopes. They finally decrease as the stretch λ_1 is getting larger. Obviously, the evolution of the $T_1 - \lambda_1$ curves is mod-

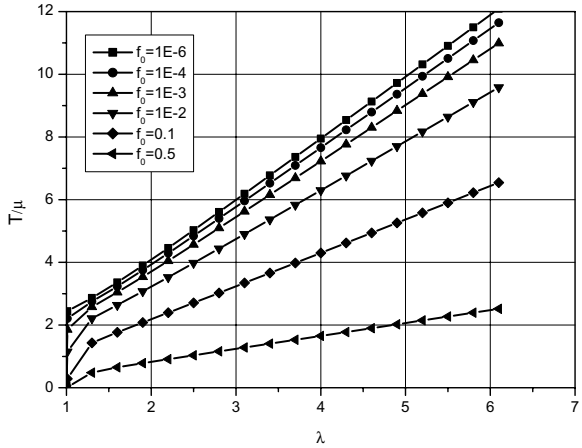

Fig. 5. Neo-Hookean laws for hydrostatic tension with different fixed initial porosities f_0.

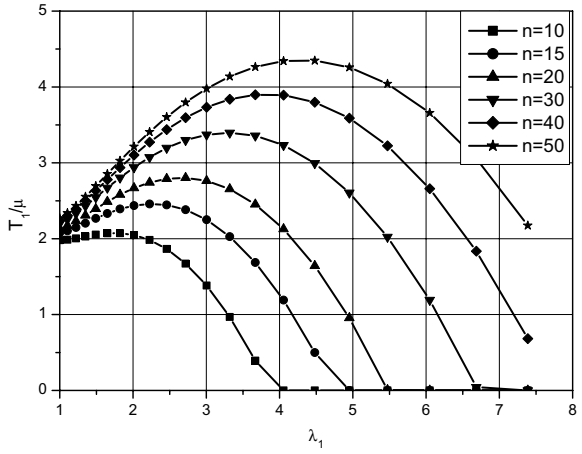

Fig. 6. Neo-Hookean laws for hydrostatic tension with growing porosity.

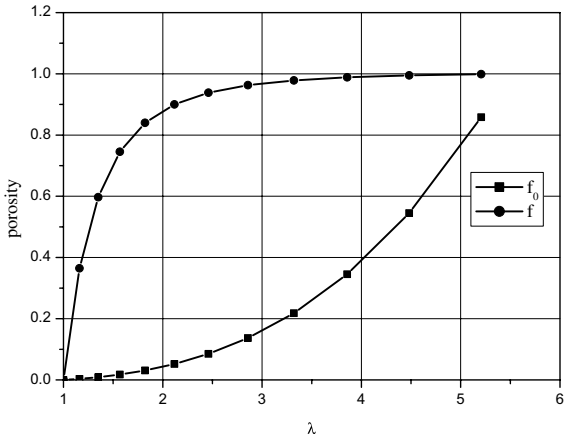

Fig. 7. Variation of f_0 and f for hydrostatic tension, $n = 20$.

ulated by the porosity growth. Thus we obtain the complete evolution curves for rubber-like materials under a hydrostatic tension due to the cavity growth.

The growing porosity f_0 (cavity in the non-deformed configuration) and the actual porosity f (in the deformed configuration) were calculated by using Eqs. (39) and (25). Fig. 7 shows their variations during the loading for $n = 20$. We can see that even though the deformed cavity increases very rapidly at the beginning of the loading, its volume in the non-deformed configuration, which represents the damage of the material, changes little. The contrary happens as the load increases.

4.4. Critical hydrostatic load for cavity growth

From the analyses performed in Section 4.3, we can observe that for fixed small initial porosities, the present model predicts nearly identical critical cavitation load with that obtained by Ball (1982), i.e., $p_c = T_1 = 2.5\mu$. However, if the cavity growth criterion (39) is introduced, this is no longer true. From Fig. 6, it is seen that the critical load of cavitation is lower than 2.5μ. In fact, there exists a critical load for cavity growth, as demonstrated in the following:

Under the critical hydrostatic pressure, the cavity evolution criterion leads to write:

$$f_0 = \frac{J-1}{\Lambda J - 1} = \frac{J-1}{\left(\frac{3n}{2}\right)^{\frac{3}{2}} J - 1}. \tag{47}$$

Introducing (47) into (46) yields

$$p_c = \lim_{\tilde{\lambda}_1 \to 1} \overline{T}_1 = \left[\frac{5}{2} - 2\left(\frac{3n}{2}\right)^{-\frac{1}{2}} - \frac{1}{2}\left(\frac{3n}{2}\right)^{-2}\right]\mu. \tag{48}$$

That is the minimal pressure required for cavity growth. This critical load is independent of the initial cavity size as this one is small enough. It is clear that when $n \to \infty$, $p_c \to 5\mu/2$, that is the critical cavitation load for incompressible neo-Hookean materials according to Ball (1982). We have to notice that this analysis on the minimal pressure is valid only for the compressible model issued from the neo-Hookean law.

4.5. Cylindrical tension

This particular stress state corresponds to axisymmetrical tension with respect to Z axis in the cylindrical frame (R,Θ,Z), i.e., $T_R = T_\Theta$ and $\lambda_R = \lambda_\Theta$. By varying the proportion of T_R/T_Z or λ_R/λ_Z, different tri-axialities can be obtained. In this work, we consider the following particular cases:

1. Imposing the stretch ratio. When the axial tension is predominant, $\lambda_Z \geqslant \lambda_R$, we can prescribe a fixed exponential ratio such that $\lambda_R = \lambda_Z^m$, $-0.5 \leqslant m \leqslant 1$. $m = 1$ corresponds to the hydrostatic tension, while $m = -0.5$ corresponds to the uniaxial tension. The $T_Z - \lambda_Z$ curves can directly be obtained from (6), namely:

$$T_Z = \frac{\mu}{2}\frac{\mathrm{d}\varphi}{\mathrm{d}J}\lambda_R\lambda_\Theta\left(\lambda_R^2 + \lambda_\Theta^2 + \lambda_Z^2\right) + \mu\varphi\lambda_Z,$$
$$T_R = \frac{\mu}{2}\frac{\mathrm{d}\varphi}{\mathrm{d}J}\lambda_R\lambda_\Theta\left(\lambda_R^2 + \lambda_\Theta^2 + \lambda_Z^2\right) + \mu\varphi\lambda_R. \tag{49}$$

By using the porosity growth criterion (39), the $T_Z - \lambda_Z$ curves were plotted for different m values, see Fig. 8. From this figure, we can remark that in strain-imposed cylindrical tension, all the $T_Z - \lambda_Z$ curves exhibit a cavity growth feature except the pure uniaxial tension. This is because in all these cases except the uniaxial tension, the imposed strain leads to a volume expansion that implies cavity growth. From this point of view, the predicted results by the present theory are physically reasonable.

2. Imposing the stress ratio. By imposing a fixed ratio T_R/T_Z, we can obtain different cylindrical tensions. It is clear that $T_R/T_Z = 0$ corresponds to the uniaxial tension whereas $T_R/T_Z = 1$ corresponds to the hydrostatic tension. We can therefore calculate the axial and radial stretches from (49). These non-linear equations were solved numerically. The obtained $T_Z - \lambda_Z$ curves for growing porosities were plotted in Fig. 9. First,

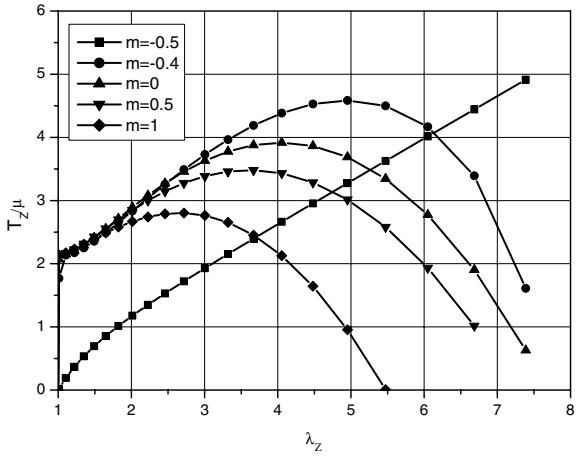

Fig. 8. Neo-Hookean laws for strain-imposed cylindrical tensions.

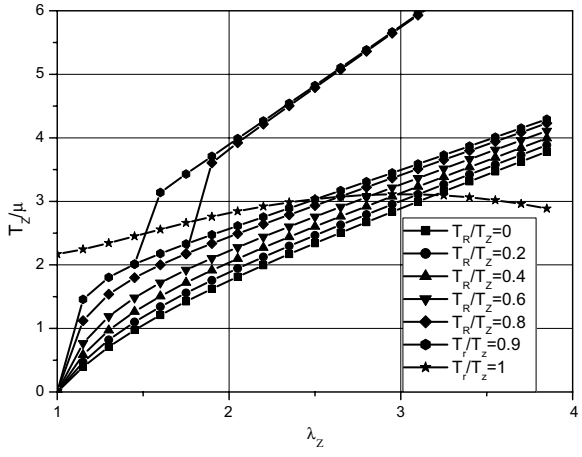

Fig. 9. Neo-Hookean laws for stress-imposed cylindrical tensions.

we observe bifurcations of the $T_Z - \lambda_Z$ curves that may represent two or more branches. The bifurcation phenomenon in solving hyperelastical problems has been pointed out and studied by numerous authors (Ball, 1982; Horgan and Abeyaratne, 1986 for examples) and will not be the central interest of this work. Second, cavitation and cavity growth occur only for pure hydrostatic tension. This is the essential divergence with the cases under strain-imposed loading. The reason for this may be that the porosity growth requires more energy consummation than the incompressible deformation as the cavities are small. When the stretches are not imposed, the material tends to adopt the configuration that consumes less energy, essentially that corresponding to an incompressible deformation.

From this analysis on the above-defined cylindrical tensions, we can remark that the present compressible model can describe efficiently the deformations of different stress states, varying from uniaxial to tri-axial tensions.

5. Experimental verification and numerical modelling

The constitutive law for the compressible materials issued from the neo-Hookean law as above-presented in detail is simple enough to give a clear outline of the new model. However, its accuracy is not sufficient to describe a real engineering rubber material. As in the case of the incompressible materials, multi-parameter models are often required. The compressible constitutive models issued from the general Rivlin's law are usually too lengthy and therefore difficult to implement in numerical models, we believe that a constitutive law with 3–5 parameters might be a good compromise between simplicity and efficiency.

The identification of the parameters in the present theory was carried out on the basis of experimental data. According to the analyses made in the preceding section, the present compressible model differs only very little from the corresponding conventional incompressible laws in the cases of uniaxial and equi-biaxial tensions. This result permits us to keep the same parameters identified in its original incompressible laws. Consequently, the identification work is considerably simplified.

In practice, uniaxial and biaxial tests are appropriate enough to correctly identify an incompressible law. However, tri-axial tests are necessary to valid the proposed model for compressible materials. In this work, the identification of the parameters was completed by means of conventional uniaxial and equi-biaxial tension tests, and tensile tests on pancake specimens were used for validation of the new model.

5.1. Experimental data base

We present briefly the experimentations carried out in this work. The material used in the experimentation was a natural rubber charged with carbon blacks.

The uniaxial tension tests were carried out with rubber sheet specimens. The displacement-controlled loading was applied until the failure of the specimen.

The equi-biaxial tension tests were performed with thin rubber sheet fixed on a specific devise and blown with water. The thickness of the rubber sheet is 2 mm. The shape of the deformed rubber sheet can be assimilated to a portion of a sphere. On the top of the sphere, the stretch state is an equi-biaxial one, i.e., $\lambda_1 = \lambda_2 = \lambda$. The pressure was applied with a low velocity until the failure of the rubber sheet.

The tension on pancake-shaped specimens is an appropriate test to produce tri-axial tension stresses in its centre part (Gent and Lindley, 1958). In our tests, the dimension of the rubber disks is of a diameter of 120 mm and a thickness of 5 mm. The rubber disk was firmly adhered on both sides to metallic armatures. The displacement-controlled loading was applied with a speed of 0.5 mm/min until the complete failure of the disk. The recorded stress–stretch diagrams for these tests are represented in Fig. 10.

5.2. Identification of compressible constitutive laws

In this work, we select three compressible models truncated from (31):

1. One-parameter model issued from the neo-Hookean law, i.e., Eq. (41).

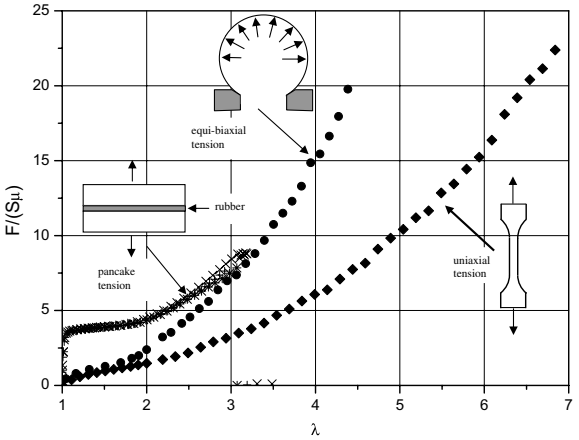

Fig. 10. Experimental results for uniaxial, equi-biaxial and pancake tests. $F/(S\mu)$ denotes the normalized nominal engineering stress.

2. One-parameter model issued from the truncated Arruda–Boyce law (1993). The 8-chain model established by Arruda and Boyce adopts the shear modulus μ as the single parameter. In this work, only the first two terms in its development were held in the construction of the compressible model, namely:

$$W = \frac{\mu}{2}\left[(I_1 - 3) + \frac{1}{20n}(I_1^2 - 9)\right]. \tag{50}$$

The homogenization of this energy density leads to obtain

$$W = \left(-\frac{3}{2} - \frac{9}{40n}\right)\mu(1 - f_0) + \frac{\mu}{2}\Phi_1 J_1 + \frac{\mu}{40n}\left[(\Phi_2 + 3\Phi_3)J_1^2 - 4\Phi_3 J_2\right]. \tag{51}$$

3. Three-parameter model issued from the truncated Rivlin's law

$$W(I_1, I_2) = C_{10}(I_1 - 3) + C_{01}(I_2 - 3) + C_{20}(I_1 - 3)^2. \tag{52}$$

Its homogenization yields

$$W = (-3C_{10} - 3C_{01} + 9C_{20})(1 - f_0) + (C_{10} - 6C_{20})\Phi_1 J_1 + C_{01}\Phi_2 J_2 + C_{20}\left[(\Phi_2 + 3\Phi_3)J_1^2 - 4\Phi_3 J_2\right]. \tag{53}$$

As argued at the beginning of this section, the parameters in these compressible models were identified by means of the uniaxial and equi-biaxial tests, on the basis of their corresponding incompressible laws. Using the standard least square procedure gives the following results: $C_{10} = 0.4\mu$, $C_{01} = 0.023\mu$, $C_{20} = 0.016\mu$, where is the shear module in the neo-Hookean law. The initial porosity chosen was $f_0 = 10\text{e}{-6}$.

For uniaxial and biaxial tensions, the $T - \lambda$ curves predicted by the new compressible models and those predicted by their corresponding incompressible laws were plotted in Figs. 11 and 12, comparing with the experimental data. We can observe that the curves predicted by these two groups of laws are completely superposed. This result justifies the identification method used in this work.

From these figures, we can also observe that the one-term model issued from the neo-Hookean law provides only a mediocre representation of the experimental results; The two-term model issued from the truncated Arruda–Boyce law gives a better result, but its accuracy is limited by the truncation. Only the three-term model issued from Rivlin's law provides a correct correlation of the experimental data.

5.3. Simple verification of the compressible models trough pancake tests

The verification of the established compressible models can be completed by means of two approaches. First, we can construct a finite element model of the pancake tests and compare the numerical result with the experimental one. This approach provides a realistic representation of the tests and therefore, a more reli-

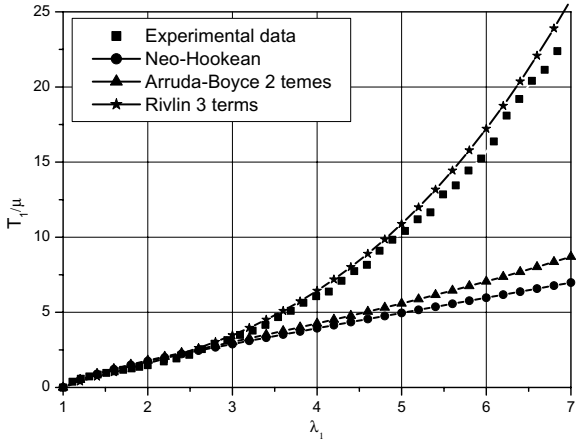

Fig. 11. Comparison between experimental data and models for uniaxial tension.

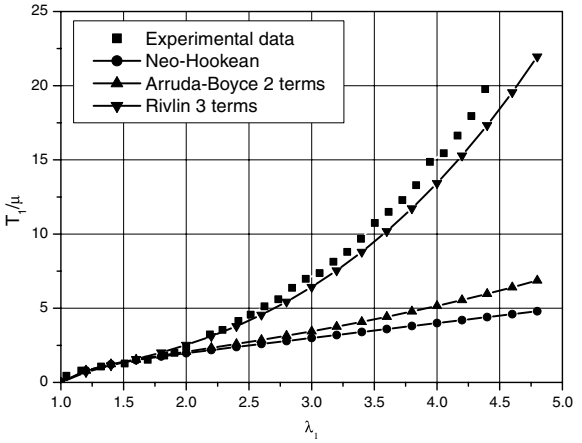

Fig. 12. Comparison between experimental data and models for equi-biaxial tension.

able result. This numerical work will be presented latter in this paper. The second approach is much simpler and can directly be accomplished by adopting a reasonable geometrical assumption. In fact, since the thickness of the rubber disk is very small (5 mm) comparing to the diameter (120 mm), the radial deformation, especially near the central part, can be neglected. As a consequence, the deformation in the disk can be considered as to be uniform, as follows:

$$\lambda_R = \lambda_\Theta = 1 \quad \lambda_Z = \frac{L}{L_0}, \tag{54}$$

where L and L_0 are, respectively, the actual and initial thickness of the disk. The engineering stress can directly be calculated according to $T_Z = \frac{\mathrm{d}W}{\mathrm{d}\lambda_Z}$. In order to better fit the experimental data, the value of the parameter n was chosen to be 25. The influence of this parameter on the predicted results will be discussed later. The obtained results for the three compressible models with cavity evolution were plotted in Fig. 13. From this figure, we can see that the one-parameter models issued from the neo-Hookean and the two-term Arruda–Boyce laws provide too conservative predictions for tensile force. The three-term model issued from the Rivlin's law, however, gives a satisfactory correlation with experimental results. From the results obtained by using this model, following remarks can be made:

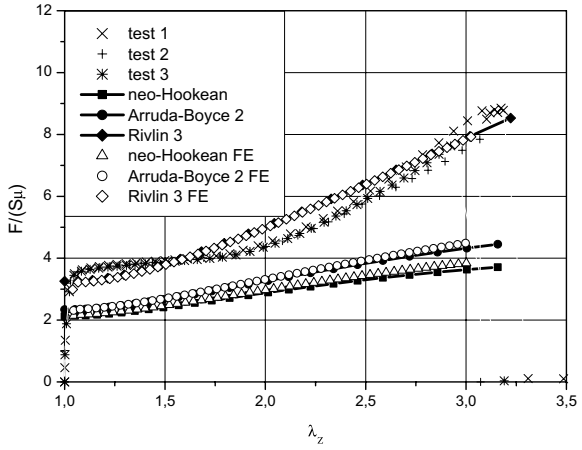

Fig. 13. Comparison between experimental data and models for pancake tests.

1. Correct critical cavity growth load (or critical cavitation load if the initial porosity f_0 is considered as to be zero) is predicted.
2. The global behaviour of rubber under tri-axial tension is correctly represented. The stretch–stress diagram predicted by the model presents a plateau immediately after the initial cavity growth, reflecting the softening behaviour due to the cavity growth. As the porosity grows, the rubber becomes increasingly compressible and then the stress tri-axiality decreases. The followed increasing curve reflects the hardening behaviour of the rubber when the stress state becomes progressively more uniaxial at high stretch level.

5.4. Numerical verification of the compressible models by finite element modelling

We performed finite element analyses in this work in order to verify the accuracy and the applicability of the above-developed constitutive model for compressible elastomers. In finite element formulations, the second Kirchhoff stress tensor $\boldsymbol{S}$ and the Green–Lagrange strain tensor $\boldsymbol{E}$ are mainly used in the description of the deformed state. Since $\boldsymbol{E}$ is related to the right Cauchy–Green stretch tensor $\boldsymbol{C}$ through (4), we have:

$$\boldsymbol{S} = 2\frac{\partial W}{\partial \boldsymbol{C}} \tag{55}$$

The rank-four tangent elastic tensor with respect to the reference configuration are deduced from

$$\boldsymbol{H} = 4\frac{\partial^2 W}{\partial \boldsymbol{C}\partial \boldsymbol{C}} \tag{56}$$

In general, no particular difficulty is presented in the implementation of the model in a finite element program even though attention should be paid in writing the lengthy expressions of the elastic tensor. Moreover, numerical precautions had to be made in order to avoid problems related to convergence or compressibility.

The pancake specimen was meshed with axi-symmetric elements and the boundary conditions corresponding to the experimentation were applied: the bottom surface was totally clamped while the top surface was clamped in the R-direction and subjected to a prescribed displacement in the Z-direction.

In Fig. 13, we represent the $T_Z - \lambda_Z$ curves obtained from the finite-element computation comparing with the simplified modelling described in the previous paragraph. Quite surprisingly, the two approaches provide nearly identical results for the three constitutive laws used. This suggests that the assumption made in (54) is quite reasonable for uniaxial tension tests with thin pancake specimens.

Fig. 14 plots the deformed specimen and the distribution of the porosity in the pancake specimens during the loading. We can observe that the distribution of the porosity f_0 is nearly uniform in the whole specimen except the region near the outer boundary. From 14, we can remark that the assumption made in (54) is globally verified except at the zone near the skin, where the strain and damage change rapidly than anywhere else in the specimen.

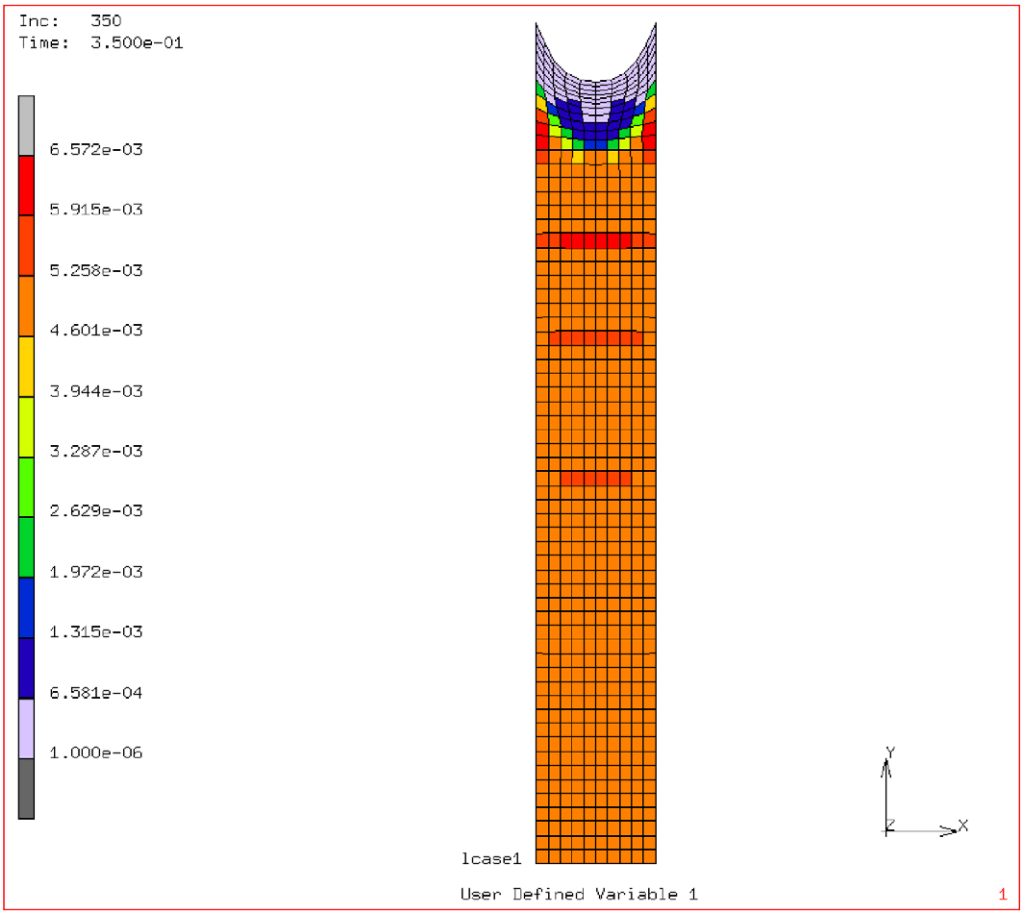

Fig. 14. Porosity distribution and deformation of the pancake specimen.

6. Discussion and conclusions

In this work, we attempted to describe the damage evolution in rubber-like material due to the cavitation and cavity growth process. By adopting the kinematics proposed by Hou and Abeyaratne (1992) for a voided element, we established a constitutive model by using a homogenization technique. As a consequence, this model, based on a micro-mechanism modelling, appears physically reasonable. Another remarkable particularity is that the volume change and the deviatory deformation of the material are coupled in this model, contrarily to traditional constitutive laws in which the two parts are often written separately.

The main advantage of this model may be its capacity to describe the behaviours of a rubber-like material for a very large range of stress states, varying from uniaxial to hydrostatic tensions. For uniaxial or biaxial tensions, in which the cavitation is not the principal source of damage, the new model is able to describe the slow cavity growth until a critical load level before the final fracture. For tri-axial tension, the limit load for cavitation and the cavity evolution can be correctly modelled. For example, we are able to draw a complete load-displacement curve for a pancake specimen under tensile loading, which agrees well with the experimental results. Another advantage may be the simplicity in the identification of the parameters. In fact, no supplementary identification procedure is needed with respect to the corresponding incompressible material, the initial parameters in Rivlin's law are sufficient in the establishment of the model.

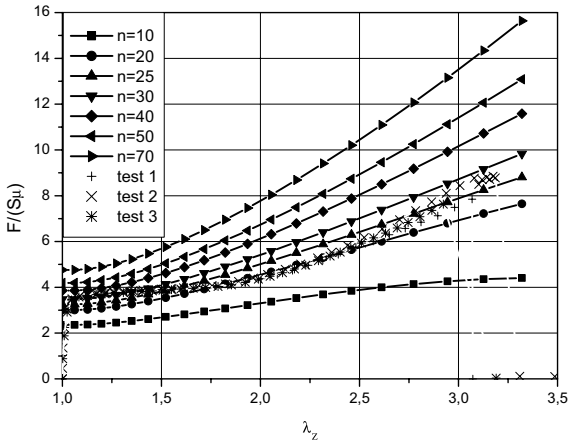

Fig. 15. $T_Z - \lambda_Z$ curves according to the three-term Rivlin's model for different values of n.

The proposed model emphasizes the importance of the parameter n, that is the number of links in a rubber molecular chain. This is the only parameter to adjust in the model. This parameter has an effective influence on the tri-axial behaviour. For example, let us consider the pancake specimens under tensile loading, studied in Section 5.2. We plot in Fig. 15 several $T_Z - \lambda_Z$ curves according the three-term Rivlin's model by using different values of n. This figure shows that the minimal tension for cavitation increases as n increases. Moreover, larger n induces higher stress responses for the same stretch level. For the present three-term model, taking $n = 25$ provides a satisfactory correlation between the model and the experiment results.

The few dissimilarities between the predicted $T_Z - \lambda_Z$ curves and the experimental data can be partially explained by the simplicity of the model since only one new parameter n was introduced as a material constant. As suggested by several authors (Johnson and Beatty, 1993; Marckmann et al., 2002), this parameter can change during the damage process. These authors described this mechanism as the breaking down of short chains such that the average chain length becomes longer. Therefore, the variation of n under tri-axial loading may be an interesting issue in the further researches.

One of questionable points in the establishment of the present model is associated to the cavity shape that would not remain exactly spherical, especially when the cavity grows. In the case when one principal strain is predominant with respect to the others, the growth of the cavity might not be spherically symmetric. The highly developed cavity may like rather a crack than a spherical void. Therefore, strictly speaking, the assumption on the spherical shape of the cavity is justifiable only when the porosity is weak and in the sense of the global effect. However, the experimental verification shows that good correlation can be obtained event in the case of large porosity. The reason for this performance may be explained by the blunt form of crack front due to the large deformation, which would considerably decrease the stress concentration level. As a consequence, the assumption on the spherically growing cavity would not introduce too important errors in the computation. Further studies are needed to highlight the influence of this assumption.

Acknowledgment

The authors gratefully acknowledge support of this work by Trelleborg Industry.

Appendix A

$$\overline{W} = C_0(1-f_0) + C_1\Phi_1 J_1 + C_2\Phi_2 J_2 + C_{20}\left[(\Phi_2+3\Phi_3)J_1^2 - 4\Phi_3 J_2\right] + C_{02}\left[(\Phi_1+3\Phi_4)J_2^2 - 4\Phi_4 J_1\right] + C_{11}\left[\Phi_5 J_1 J_2 + \Phi_6\right]$$

where

$$C_0 = -3C_{10} - 3C_{01} + 9C_{20} + 9C_{02} + 9C_{11}$$
$$C_1 = C_{10} - 6C_{20} - 3C_{11}$$
$$C_2 = C_{01} - 6C_{02} - 3C_{11}$$
$$J_1 = \bar{I}_1 J^{-\frac{2}{3}} \quad J_2 = \bar{I}_2 J^{-\frac{4}{3}}$$
$$\Phi_1(f_0, J) = J^{-\frac{1}{3}}(2J-1) - f_0\left(1 + \frac{J-1}{f_0}\right)^{-\frac{1}{3}}\left(1 + 2\frac{J-1}{f_0}\right)$$
$$\Phi_2(f_0, J) = J^{\frac{1}{3}}(2-J) - f_0\left(1 + \frac{J-1}{f_0}\right)^{\frac{1}{3}}\left(1 - \frac{J-1}{f_0}\right)$$
$$\Phi_3(f_0, J) = \frac{J-1}{25}\left[J^{-\frac{5}{3}}(1 + 5J - 5J^2) - \frac{1 - 5(J-1)/f_0 - 5(J-1)^2/f_0^2}{[1 + (J-1)/f_0]^{\frac{5}{3}}}\right]$$
$$\Phi_4(f_0, J) = \frac{J-1}{25}\left[J^{-\frac{1}{3}}(5 - 5J + J^2) + \frac{1 + 7(J-1)/f_0 + (J-1)^2/f_0^2}{[1 + (J-1)/f_0]^{\frac{1}{3}}}\right]$$
$$\Phi_5(f_0, J) = (1 - f_0) + \frac{4}{15}(J-1)\left[2\ln\left(\frac{J - 1 + f_0}{Jf_0}\right) + (J-1)\left(\frac{1 - f_0}{f_0}\right)\right]$$
$$\Phi_6(f_0, J) = -\frac{2}{5}(J-1)\left[2\ln\left(\frac{J - 1 + f_0}{Jf_0}\right) + (J-1)\left(\frac{1 - f_0}{f_0}\right)\right]$$

References

Arruda, E.M., Boyce, M.C., 1993. A three-dimensional constitutive model for the large stretch behaviour of elastomers. J. Mech. Phys. Solids 41, 389–412.

Attard, M.M., Hunt, G.W., 2002. Hyperelastic constitutive modelling under finite strain. Int. J. Solids Struct. 41, 5327–5350.

Ball, J.M., 1982. Discontinuous equilibrium solutions and cavitation in nonlinear elasticity. Phil. Trans. R. Soc. Lond. A 306, 557–611.

Bathias, C., Legorju, C., Chuming, L.U., Menabeuf, L., 1996. Fatigue crack growth damage in elastomeric materials. In: Elastomeric materials, ASTM, STP, 505–513.

Bischoff, J.E., Arruda, E.M., Grosh, K., 2000. A new constitutive model for the compressibility of elastomers at finite deformations. Rubber Chem. Tech. 74, 541–559.

Biva, S., 1995. Critical stretch for formation of a cylindrical void in a compressible hyperelastic material. Int. J. Non-Linear Mech. 30, 899–914.

Blatz, P.J., Ko, W.L., 1962. Application of finite elasticity to deformation of rubber materials. Trans. Soc. Rheol. 6, 223.

Chang, w.J., Pan, J., 2001. Cavitation instability in rubber with consideration of failure. J. Materials Sci. 36, 1901–1909.

Diani, J., 1999. Contribution à l'étude du comportement élastique et de l'endommagement des matériaux élastomères. PhD thesis, Ecole Normale Supérieure de Cachan, Cachan, France.

Dorfmann, A., 2003. Stress softening of elastomers in hydrostatic tension. Acta Mechanica 165, 117–137.

Dorfmann, A., Burtscher, S., 2000. Aspects of cavitation damage in seismic bearings. ASCE J. Struct. Eng. 126, 573–579.

Dorfmann, A., Fuller, K.N.G., Ogden, R.W., 2002. Shear, compressive and dilatational response of rubberlike solids subject to cavitation damage. Int. J. Solids Struct. 39, 1845–1861.

Fond, C., Lobbrecht, A., Schirrer, R., 1996. Polymers toughened with rubber microspheres: an analytical solution for stresses and strains in the rubber particles at equilibrium and rupture. Int. J. Fracture 77, 141–159.

Ganghoffer, J.F., Schultz, J., 1995. A new theoretical approach to cavitation in rubber. Rubber Chem. Tech. 68, 757–772.

Gent, A.N., Lindley, P.B., 1958. Internal rupture of bonded rubber cylinders in tension. Proc. R Soc. Lond. A249, 195–205.

Gent, A.N., Wang, C., 1991. Fracture mechanics and cavitation in rubber-like solids. J. Mater. Sci. 26, 3392–3395.

Horgan, C.O., Abeyaratne, R., 1986. A bifurcation problem for a compressible nonlinearly elastic medium: growth of a micro-void. J. Elasticity 16, 189–200.

Hou, H.S., Abeyaratne, R., 1992. Cavitation in elastic and elastic-plastic solids. J. Mech. Phys. Solids 40, 571–722.

Hou, H.S., Zhang, Y., 1992. The effect of axial stretch on cavitation in an elastic cylinder. Int. J. Non-Linear Mech. 25, 715–722.

Johnson, M.A., Beatty, M.F., 1993. The Mullins effect in uniaxial extension and its influence on transverse vibration of rubber string. Continuum Mech. Thermodyn. 5, 83–115.

Kakavas, P.A., Chang, W.V., 1991. Acoustic emission in bonded elastomeric discs subjected to uniform tension. J. Appl. Pol. Sci. 42, 1997.

Kakavas, P.A., Chang, W.V., 1992. Acoustic emission in bonded elastomeric discs subjected to compression. J. Appl. Pol. Sci. 42, 865.

Legorju-jago, K., Bathias, C., 2002. Fatigue initiation and propagation in natural and synthetic rubbers. Int. J. Fatigue 24, 85–92.
Lindsey, G.H., 1967. Triaxial fracture studies. J. Appl. Phys. 38, 4843–4852.
Mark, J.E., Erman, B., 1988. Rubberlike Elasticity. Willey, New York.
Marckmann, G., Verron, E., Gornet, L., Chagnon, G., Charrier, P., Fort, P., 2002. A theory of network alteration for the Mullins effect. J. Mech. Phys. Solids 50, 2011–2028.
Ogden, R.W., 1972. Large deformation isotropic elasticity: on the correlation of theory and experiment for compressible rubber-like solids. Proc. R Soc. Lond. A328, 567–583.
Ogden, R.W., 1976. Volume changes associated with the deformations: application to rubber-like solids. J. Mech. Phys. Solids 24, 323–338.
Ogden, R.W., Roxburgh, D.G., 1999. A pseudo-elastic model for the Mullins effect in filled. Proc. R Soc. Lond. A455, 12861–12878.
Polignone, D.A., Horgan, C.O., 1993. Cavitation for incompressible anisotropic nonlinearly elastic spheres. J. Elasticity 33, 27–65.
Shang, X.C., Cheng, C.J., 2001. Exact solution for cavitated bifurcation for compressible hyperelastic materials. Int. J. Eng. Sci. 39, 1101–1117.
Simo, J.C., Pister, K.S., 1984. Remarks on rate constitutive equations for finite deformation problems: computational implications. Computer Meth. Appl. Mech. Eng. 46, 201–215.
Steenbrink, A.C., Van der Giessen, E., 1999. On cavitation, post-cavitation and yield in amorphous polymer-rubber blends. J. Mech. Phys. Solids 47, 843–876.
Treloar, L.R., 1975. The Physical of Rubber Elasticity. Clareendon Press, Oxford.
Voigt, W.U., 1889. ber die Beziehung zwischen den beiden Elastizita tskonstanten isotroper Korper. Wied Ann Physik 38, 573–587.
Williams, M.L., Schapery, R.A., 1965. Spherical flaw instability in hydrostatic tension. Int. J. Fracture Mech. 1, 64–71.